Article

MMS

Mathematics and Mechanics of Solids
1–16

DOI: 10.1177/1081286519856062
journals.sagepub.com/home/mms
SAGE

Elastic buckling analysis of an embedded infinitely long rod under combined axial and torsional loads

Dong Wang
Robotics Institute, and State Key Laboratory of Mechanical System and Vibration, School of Mechanical Engineering, Shanghai Jiao Tong University, Shanghai, China

Mao See Wu
School of Mechanical and Aerospace Engineering, Nanyang Technological University, Singapore

Received 1 February 2019; accepted 17 May 2019

Abstract
In this paper, expressions for the critical axial–torsional loads are derived for the buckling of an elastic rod embedded in an elastic medium. The derivation is based on the assumption that the deforming rod encounters a response force from the surrounding medium, and a first-order perturbation analysis of the governing equilibrium equations. It is shown that a dimensionless universal buckling relationship, independent of material and geometry, exists between the critical axial load, both in compression and tension, and the critical torsional load. A reducing axial compression, or an increasing axial tension, enhances the critical torsional load. In addition, two different mode shapes are predicted for the same critical combined loads, and the buckled shapes are generally three-dimensional.

Keywords
Buckling, embedded rod, axial and torsional loads

1. Introduction

The structure of a thin elastic filament embedded in a soft medium is ubiquitous in nature and engineering. Examples exist in all scales including: DNA strands coiled in a cell [1, 2], microtubules supported by cytoplasm in living cells [3–7], bacteria swimming by their flagellar filaments in an aqueous environment [8, 9], plant roots growing in soil [10], electrodes embedded in brain tissues for deep brain simulations [11], and pipelines on the seabed [12, 13].

The buckling behaviors of these structures have drawn considerable attention in recent years, particularly regarding the effect of the surrounding elastic medium on the buckling of the rod. It has been shown that the elastic matrix can help prevent rod buckling and, hence, the rod could sustain significantly higher loadings [14, 15].

A number of models have been developed to investigate the buckling of rods in a soft medium. For example, an early work suggests that the buckling of compressively loaded microtubules within a

Corresponding author:
Dong Wang, Robotics Institute, and State Key Laboratory of Mechanical System and Vibration, DongChuan Road 800, School of Mechanical Engineering, Shanghai Jiao Tong University, Shanghai 200240, China.
Email: wang_dong@sjtu.edu.cn

Table 1. Summary of previous and current works on the critical buckling loads P_c and T_c of a long rod under different types of loading with and without medium.

	Pure axial load P_c	Pure torsional load T_c	Combined P_c and T_c
Without medium	Euler buckling $P_c = \frac{\pi^2 EI}{L^2}$; immediately buckles for long rod	Immediately buckles for long rod	$P_c = \frac{T_c^2}{4EI}$ (see [25–27])
With medium	$P_c = -2\sqrt{EI\alpha}$ (see [3, 18])	No analytical results (to the best of the authors' knowledge)	No analytical results (to the best of the authors' knowledge)
Without medium (current work)	Immediately buckles for long rod	Immediately buckles for long rod	$P_c = \frac{T_c^2}{4EI}$
With medium (current work)	$P_c = -2\sqrt{EI\alpha}$	$T_c = \pm \frac{4\left(EI^3\alpha\right)^{1/4}}{3^{3/4}}$	$T_c = \pm \frac{1}{3}\sqrt{\frac{2}{3}}\sqrt{\frac{-P_c^3 + 36EIP_c\alpha + \sqrt{\left(P_c^2 + 12EI\alpha\right)^3}}{\alpha}}$

network of intermediate filaments may be prevented [16]. A later experimental and theoretical work also shows that microtubules in cell cytoskeleton could withstand significantly higher compressive force [3]. Subsequently, the force propagation along an elastic rod embedded in a nonlinear elastic matrix has also been examined by taking into account both linear and nonlinear effects [17]. Through both experiments and theory, the buckling amplitude is shown to decay exponentially away from the ends of the rod. More recently, Su et al. [18] shows experimentally and theoretically that a compressed rod embedded in a soft matrix could exhibit both in-plane and out-of-plane shapes in the post-buckling regime. Lim [19] has also studied the buckling behavior of an elastic rod with intrinsic curvature and twist in a viscous fluid, whereas Wang and Van der Heijden [20] have studied the localized buckling of subsea pipelines subject to nonlinear soil resistance.

Most of the studies have considered compressive force as the applied loading. However, this assumption is typically an oversimplification. For example, a torsional stress can be generated on DNA strands as proteins move along them [1, 21]; the flow of intracellular fluid could induce torsional moment on microtubules in cells [22, 23]; shear stress is produced due to the anisotropic growth of plant roots [10]; a torsional moment on pipelines on the seabed can also be induced by a lateral current [24]. However, the effects of an ambient elastic medium on the buckling of a rod under pure torsion or combined axial and torsional loading remain poorly understood, as highlighted by the summary of previous works given in Table 1.

The buckling behavior of a rod under combined torsion and axial loading *without* lateral restraint has been studied quite extensively. For example, the critical point at which a rod under combined torsion and axial loading becomes unstable has been obtained from a linear eigenvalue analysis [25–27]. The helical buckling of a conducting rod under compression, twist, or whirl generated by magnetic field has also been investigated [28, 29]. A general framework for studying the static and dynamic behavior of a rod under torsion and axial loading has also been proposed using the Kirchhoff rod theory [30]. In these studies, however, the effect of the surrounding soft matrix was not incorporated.

For finite-length rods, the boundary conditions also govern the buckling load. The critical buckling load for beam with several types of boundary conditions (pinned or clamped) was first derived in [31] and further refined in [32]. Later, the effect of boundary conditions on the critical buckling load and buckling modes has been studied extensively for a rod subjected to different loadings and using different methods [27, 33]. For example, it was found that under a coat hanger boundary condition, a rod buckles exclusively into a helix and the critical loads can be obtained explicitly unlike the case with welded boundary condition [29]. Unlike the twisting instability evolving from a kink to a knot for a long cylinder rod under pure torsion, wrinkles will occur on a short soft cylinder due to a geometric constraint of zero displacement of the axis of the cylinder and this phenomenon was studied by using the theory of incremental elastic deformation [34]. The buckling behaviors of hyperelastic cylinder tubes were derived within the framework of nonlinear elasticity and the results show that boundary effect can affect the transition between buckling and barreling [35].

In this paper, the analytical solutions of the critical buckling load are obtained for a infinitely long rod embedded in an elastic medium under pure axial loading, pure torsion, and combined torsion–axial

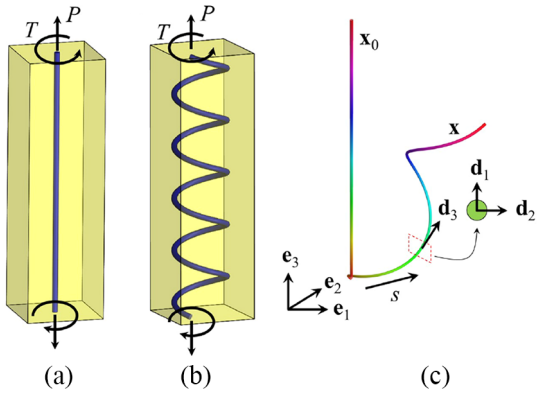

Figure 1. Schematics of the shape of a rod embedded in elastic medium (a) before and (b) after buckling. (c) Before buckling, the configuration of the rod is represented by $\mathbf{x}_0$; after buckling, the rod is represented by a curve $\mathbf{x}(s)$ and by a local director basis $(\mathbf{d}_1, \mathbf{d}_2, \mathbf{d}_3)$.

loading. The rod is assumed to be infinitely long and boundary conditions are not required. The infinitely long assumption is reasonable in cases when the length dimension is considerably greater than the radius. This assumption has also been made in previous works [19, 36–38], where the DNA molecules, bacterial flagellar filaments, micro-tubules, and seabed pipelines are all considered long rods. The analysis is based on a perturbation scheme of Kirchhoff's rod theory. The work focuses on the effect of the elastic medium on the critical buckling load and the corresponding shape.

2. Analytical model

2.1. Kirchhoff model of a rod in an elastic medium

We consider a infinitely long thin elastic rod with a circular cross-section, embedded in an elastic medium under a combined axial force P and torsional moment T as shown in Figure 1(a). Also shown in the figure is a three-dimensional (3D) Cartesian basis with basis vectors $(\mathbf{e}_1, \mathbf{e}_2, \mathbf{e}_3)$. A positive P means a tensile force, whereas a negative P represents compression. The rod is assumed to be inextensible and unshearable in the Kirchhoff theory. At the critical loading, the initially straight configuration is no longer stable and the rod will buckle as shown in Figure 1(b). The centerline of the rod is described by the position vector $\mathbf{x}(s)$, where s is the path variable as shown in Figure 1(c). Note that due to the inextensible assumption, the total length L of the rod does not change during deformation, so that $s \in [0, L]$. In addition, a local director basis

$$(\mathbf{d}_1, \mathbf{d}_2, \mathbf{d}_3) = (\mathbf{d}_1(s), \mathbf{d}_2(s), \mathbf{d}_3(s)) \tag{1}$$

is associated with the rod as shown in Figure 1(c). The vector $\mathbf{d}_3$ is the unit tangent to the curve,

$$\mathbf{d}_3(s) = \mathbf{x}', \tag{2}$$

where the prime symbol denotes differentiation with respect to s. For the sake of simplicity, $(\mathbf{d}_1, \mathbf{d}_2, \mathbf{d}_3)$ in the undeformed state is chosen to be along $(\mathbf{e}_1, \mathbf{e}_2, \mathbf{e}_3)$.

For a rod under moment and axial loadings in an elastic medium, the fundamental equations of equilibrium are [39]

$$\mathbf{F}' + \mathbf{P} = 0, \tag{3}$$

$$\mathbf{M}' + \mathbf{d}_3 \times \mathbf{F} = 0, \tag{4}$$

where $\mathbf{F}(s)$ and $\mathbf{M}(s)$ are the force and moment acting on the rod. Furthermore, $\mathbf{P}$ is the distributed force per unit length on the rod applied by the elastic medium:

$$\mathbf{P} = -\alpha(\mathbf{x} - \mathbf{x}_0), \tag{5}$$

where α is the stiffness of the elastic medium and $\mathbf{x}_0$ is the undeformed shape of the rod given by $\mathbf{x}_0 = 0\mathbf{e}_1 + 0\mathbf{e}_2 + s\mathbf{e}_3$. The rod and surrounding elastic medium are assumed to be perfectly bonded. As the rod deforms, it pushes the surrounded elastic medium and receives a response force from the elastic medium whose magnitude is assumed to be proportional to the displacement of the elastic medium. Implicitly, an assumption has been made that the rod deformation encounters negligible moment resistance from the surrounding medium. Furthermore, P_1 and P_2 in $\mathbf{P} = \{P_1, P_2, P_3\}^{\mathrm{T}}$ represent the reactive transverse forces acting on the rod and distorting it, while P_3 represents the force along the axial direction. Conceivably, the stiffness α would be different along the transverse direction (medium is being pushed/pulled) and the axial direction (medium provides tangential resistance to the rod at the interface). However, in the Kirchhoff assumption the rod is inextensible, i.e., $x_3 = x_{03} = s$ in the first-order theory and $P_3 = 0$ by Equation (5), so that it is not necessary to use an anisotropic α. In other words, the surrounding medium only transmits transverse forces to the rod.

The force and position vectors $\mathbf{F}$ and $\mathbf{x}$ can be expressed locally in terms of the director basis, i.e.,

$$\mathbf{F} = f_1(s)\mathbf{d}_1 + f_2(s)\mathbf{d}_2 + f_3(s)\mathbf{d}_3, \tag{6}$$

$$\mathbf{x} = x_1(s)\mathbf{d}_1 + x_2(s)\mathbf{d}_2 + x_3(s)\mathbf{d}_3. \tag{7}$$

The relationship between the moment $\mathbf{M}$ and the curvatures of the rod takes the following linear form:

$$\mathbf{M} = EI\kappa_1\mathbf{d}_1 + EI\kappa_2\mathbf{d}_2 + GJ\kappa_3\mathbf{d}_3, \tag{8}$$

where E is the Young modulus, G the shear modulus, I the moment of area about a diameter, and J the polar moment about the longitudinal axis. For a rod with circular cross-section, $J = 2I$. In addition, κ_i are the components of the curvature vector $\boldsymbol{\kappa} = \kappa_1\mathbf{d}_1 + \kappa_2\mathbf{d}_2 + \kappa_3\mathbf{d}_3$. Here, κ_1 and κ_2 are the material curvatures and κ_3 is the twist density. Essentially, they express how much the frame $(\mathbf{d}_1, \mathbf{d}_2, \mathbf{d}_3)$ rotates about the directions $\mathbf{d}_1$, $\mathbf{d}_2$, and $\mathbf{d}_3$. Thus, the derivatives of the director basis can be expressed as $\mathbf{d}_i' = \boldsymbol{\kappa} \times \mathbf{d}_i$, $i = 1, 2, 3$, so that

$$\begin{aligned} \mathbf{d}_1' &= -\kappa_2\mathbf{d}_3 + \kappa_3\mathbf{d}_2, \\ \mathbf{d}_2' &= \kappa_1\mathbf{d}_3 - \kappa_3\mathbf{d}_1, \\ \mathbf{d}_3' &= -\kappa_1\mathbf{d}_2 + \kappa_2\mathbf{d}_1. \end{aligned} \tag{9}$$

Equations (3) and (4) are essentially the governing equations. Substituting Equation (7) and $\mathbf{x}_0$ into the differentiated form of Equation (3) yields

$$\mathbf{F}'' = \frac{d(\alpha(\mathbf{x} - \mathbf{x}_0))}{ds} = \alpha(\mathbf{d}_3 - \mathbf{e}_3), \tag{10}$$

and upon further differentiation,

$$\mathbf{F}''' = \alpha(\mathbf{d}_3') = \alpha(-\kappa_1\mathbf{d}_2 + \kappa_2\mathbf{d}_1). \tag{11}$$

Differentiating Equation (6) three times on both sides while using the rules given in Equation (9), and comparing it with Equation (11), the following three governing equations (12), (13), and (14) can be obtained in the three director basis directions $(\mathbf{d}_1, \mathbf{d}_2, \mathbf{d}_3)$. Specifically, denoting the prime symbol as derivative with respect to s, for example $f_1''' = d^3 f_1/ds^3$, $\kappa_3' = d\kappa_3/ds$, etc., the three equations can be written as

$$f_1''' - 3(\kappa_3' f_2' - \kappa_2' f_3') - 3(\kappa_2 F_{21} + \kappa_3 F_{31}) + (f_2 G_{21} + f_3 G_{31}) = \alpha\kappa_2, \tag{12}$$

$$f_2''' - 3(\kappa_1' f_3' - \kappa_3' f_1') - 3(\kappa_1 F_{12} + \kappa_3 F_{32}) + (f_1 G_{12} + f_3 G_{32}) = -\alpha\kappa_1, \tag{13}$$

$$f_3''' - 3(\kappa_2' f_1' - \kappa_1' f_2') - 3(\kappa_1 F_{13} + \kappa_2 F_{23}) + (f_1 G_{13} + f_2 G_{23}) = 0, \tag{14}$$

where $F_{21}, F_{31}, F_{12}, F_{32}, F_{13}, F_{23}$ and $G_{21}, G_{31}, G_{12}, G_{32}, G_{13}, G_{23}$ are given in Appendix A1. The additional three equations can be obtained by substituting Equations (6), (8), and (9) into Equation (4), leading to

$$-f_2 + (-EI + GJ)\kappa_2\kappa_3 + EI\kappa_1{}' = 0, \tag{15}$$

$$f_1 + (EI - GJ)\kappa_1\kappa_3 + EI\kappa_2{}' = 0, \tag{16}$$

$$GJ\kappa_3{}' = 0. \tag{17}$$

In principle, the six governing equations (12)–(17) can be used to solve for the six unknowns. In the following, a perturbation approach is used to analyze the buckling of the rod. The objective is to derive analytical expressions for the critical buckling loads under combined torsion and axial loading. The possible corresponding mode shapes are also predicted.

2.2. Buckling analysis

In order to find the criterion for the buckling of the rod, a perturbation theory is used. By expanding the variables $\mathbf{d}_i$ as power series in a perturbation parameter ε, $\mathbf{d}_i$ can be written as

$$\mathbf{d}_i = \mathbf{d}_i^{(0)} + \varepsilon\mathbf{d}_i^{(1)} + O(\varepsilon^2), \quad i = 1, 2, 3, \tag{18}$$

where $\mathbf{d}_i^{(0)}$ denote the reference (unperturbed) director basis and ε is a marker indicating the perturbation order. The orthonormality condition requires $\mathbf{d}_i \cdot \mathbf{d}_j = \delta_{ij}$, which implies $\mathbf{d}_i^{(0)} \cdot \mathbf{d}_j^{(0)} = \delta_{ij}$ and $(\mathbf{d}_i^{(0)} + \varepsilon\mathbf{d}_i^{(1)}) \cdot (\mathbf{d}_j^{(0)} + \varepsilon\mathbf{d}_j^{(1)}) = \delta_{ij}$. The perturbed basis $\mathbf{d}_i^{(1)}$ can be expressed in terms of the unperturbed basis $\mathbf{d}_i^{(0)}$ as

$$\mathbf{d}_i^{(1)} = \sum_{j=1}^{3} A_{ij}\mathbf{d}_j^{(0)}, \tag{19}$$

where A_{ij} are the components of the antisymmetric matrix $\mathbf{A}$

$$\mathbf{A} = \begin{pmatrix} 0 & \beta_3 & -\beta_2 \\ -\beta_3 & 0 & \beta_1 \\ \beta_2 & -\beta_1 & 0 \end{pmatrix}. \tag{20}$$

In the above equation, $\beta_1, \beta_2, \beta_3$ are three unknowns to be determined. The twist vector $\boldsymbol{\kappa} = \kappa_1\mathbf{d}_1 + \kappa_2\mathbf{d}_2 + \kappa_3\mathbf{d}_3$ can then be written in terms of the perturbed variables as [28, 30, 40]

$$\mathbf{K} = \mathbf{K}^{(0)} + \mathbf{K}^{(1)} + O(\varepsilon^2) = \mathbf{B}^{\mathrm{T}}\left(\mathbf{B}\mathbf{K}^{(0)} + \frac{\partial\mathbf{B}}{\partial s}\right), \tag{21}$$

where

$$\begin{aligned}
\mathbf{K} &= \begin{pmatrix} 0 & \kappa_3 & -\kappa_2 \\ -\kappa_3 & 0 & \kappa_1 \\ \kappa_2 & -\kappa_1 & 0 \end{pmatrix}, \\
\mathbf{K}^{(0)} &= \begin{pmatrix} 0 & \kappa_3^{(0)} & -\kappa_2^{(0)} \\ -\kappa_3^{(0)} & 0 & \kappa_1^{(0)} \\ \kappa_2^{(0)} & -\kappa_1^{(0)} & 0 \end{pmatrix}, \\
\mathbf{K}^{(1)} &= \begin{pmatrix} 0 & \kappa_3^{(1)} & -\kappa_2^{(1)} \\ -\kappa_3^{(1)} & 0 & \kappa_1^{(1)} \\ \kappa_2^{(1)} & -\kappa_1^{(1)} & 0 \end{pmatrix},
\end{aligned} \tag{22}$$

$\mathbf{B} = \mathbf{I} + \varepsilon\mathbf{A} + O(\varepsilon^2)$ and $\mathbf{I}$ is the identity. The zeroth- and first-order terms of $\kappa_1, \kappa_2, \kappa_3$ can thus be obtained by expanding Equation (21). By combining Equations (9) and (19), the nine components and their derivatives of the director basis are described by only three independent parameters $\beta_1, \beta_2, \beta_3$. Substituting Equation (18) into the six governing equations (12)–(17), the Kirchhoff equations in the zeroth and first orders can be obtained.

For the zeroth-order equations, only trivial solution exist, i.e.,

$$(\kappa_1^{(0)}, \kappa_2^{(0)}, \kappa_3^{(0)}) = (0, 0, \tau), (f_1^{(0)}, f_2^{(0)}, f_3^{(0)}) = (0, 0, P), \tag{23}$$

where $\tau = T/GJ$ and T is the torsional moment or torque. This solution means that the rod remains straight. Next, we focus on the first-order equilibrium equation and express the solution of the first order as

$$(\beta_1^{(1)}, \beta_2^{(1)}, \beta_3^{(1)}, f_1^{(1)}, f_2^{(1)}, f_3^{(1)}) = \mathbf{c}e^{iw_n s}, \tag{24}$$

where $\mathbf{c} = (c_1, c_2, c_3, c_4, c_5, c_6)$ is the amplitude vector, w_n is the wave number of the corresponding mode. The six governing equations Equations (12)–(17) contains six unknowns $\kappa_1, \kappa_2, \kappa_3, f_1, f_2, f_3$. The zeroth- and first-order terms of $\kappa_1, \kappa_2, \kappa_3$ are given in Equation (A15) in Appendix A2, while the zeroth- and first-order terms of f_1, f_2, f_3 are given by Equations (23) and (24). Substituting the zeroth- and first-order terms of $\kappa_1, \kappa_2, \kappa_3, f_1, f_2, f_3$ into the six Governing equations and keep only the terms up to first order, we can obtain the first-order Kirchhoff equations as

$$\mathrm{e}^{\mathrm{i}sw_n}\varepsilon(c_5(\tau^3 + 3\tau w_n^2) - \mathrm{i}w_n(-2\mathrm{i}Pc_1\tau w_n + c_4(3\tau^2 + w_n^2) + c_2(\alpha + P(\tau^2 + w_n^2)))) = 0, \tag{25}$$

$$\mathrm{i}\mathrm{e}^{\mathrm{i}sw_n}\varepsilon(\mathrm{i}c_4(\tau^3 + 3\tau w_n^2) + w_n(2\mathrm{i}Pc_2\tau w_n - c_5(3\tau^2 + w_n^2) + c_1(\alpha + P(\tau^2 + w_n^2)))) = 0, \tag{26}$$

$$-\mathrm{i}\mathrm{e}^{\mathrm{i}sw_n}\varepsilon c_6 w_n^3 = 0, \tag{27}$$

$$-\mathrm{e}^{\mathrm{i}sw_n}\varepsilon(c_5 + w_n(\mathrm{i}(EI - GJ)c_2\tau + EIc_1 w_n)) = 0, \tag{28}$$

$$\mathrm{e}^{\mathrm{i}sw_n}\varepsilon(c_4 + w_n(\mathrm{i}(EI - GJ)c_1\tau - EIc_2 w_n)) = 0, \tag{29}$$

$$-\mathrm{e}^{\mathrm{i}sw_n}\varepsilon GJc_3 w_n^2 = 0. \tag{30}$$

The first-order equilibrium equations can be rewritten in matrix form as

$$\mathbf{L}\mathbf{c} = 0, \tag{31}$$

where $\mathbf{L}$ is given by

$$\mathbf{L} = \begin{pmatrix} -2P\tau w_n^2 & -\mathrm{i}\alpha w_n - \mathrm{i}P\tau^2 w_n - \mathrm{i}Pw_n^3 & 0 & -3\mathrm{i}\tau^2 w_n - \mathrm{i}w_n^3 & \tau^3 + 3\tau w_n^2 & 0 \\ \mathrm{i}\alpha w_n + \mathrm{i}P\tau^2 w_n + \mathrm{i}Pw_n^3 & -2P\tau w_n^2 & 0 & -\tau^3 - 3\tau w_n^2 & -3\mathrm{i}\tau^2 w_n - \mathrm{i}w_n^3 & 0 \\ 0 & 0 & 0 & 0 & 0 & -\mathrm{i}w_n^3 \\ -EIw_n^2 & \mathrm{i}(-EI + GJ)\tau w_n & 0 & 0 & -1 & 0 \\ \mathrm{i}(EI - GJ)\tau w_n & -EIw_n^2 & 0 & 1 & 0 & 0 \\ 0 & 0 & -GJw_n^2 & 0 & 0 & 0 \end{pmatrix}. \tag{32}$$

In general, $\mathbf{L}$ is non-singular, so that only the trivial solution exists. Buckling occurs when $\mathrm{Det}(\mathbf{L}) = 0$, which results in

$$\left(\alpha + EI(\tau - w_n)^4 + (\tau - w_n)^2(P + GJ\tau(-\tau + w_n))\right) \times \left(-\alpha - (\tau + w_n)^2\left(P - GJ\tau(\tau + w_n) + EI(\tau + w_n)^2\right)\right) = 0. \tag{33}$$

Thus, P can be solved as

$$P = -\frac{\alpha + (\tau - w_n)^3((EI - GJ)\tau - EIw_n)}{(\tau - w_n)^2}, \tag{34}$$

or

$$P = -\frac{\alpha + (\tau + w_n)^3((EI - GJ)\tau + EIw_n)}{(\tau + w_n)^2}. \tag{35}$$

2.3 Particular cases

In the following, the minimum or critical buckling loads P_c and τ_c (or T_c) for three particular cases are derived. To avoid cumbersome terminology, these critical loads will be denoted simply as P and τ (or T).

2.3.1 Rod buckling under pure axial loading. If the rod is under a pure compressive force, the torque $T = 0$ and, hence, $\tau = 0$. Equations (34) and (35) reduce to the same expression:

$$P = -(EIw_n{}^2 + \frac{\alpha}{w_n{}^2}). \tag{36}$$

The critical compressive load can then be calculated by minimizing the magnitude of P, yielding

$$P = -2\sqrt{EI\alpha}, \tag{37}$$

and the corresponding wave number is given by

$$w_n = \left(\frac{\alpha}{EI}\right)^{1/4}. \tag{38}$$

These results of rod buckling in an elastic medium under a pure compressive force are the same as those obtained in other works [3, 18].

2.3.2 Rod buckling under pure torsion. If the rod is under a pure torsional moment, the applied force $P = 0$. Thus, Equations (34) and (35) reduce to

$$-\frac{\alpha + (\tau - w_n)^3((EI - GJ)\tau - EIw_n)}{(\tau - w_n)^2} = 0, \tag{39}$$

or

$$-\frac{\alpha + (\tau + w_n)^3((EI - GJ)\tau + EIw_n)}{(\tau + w_n)^2} = 0. \tag{40}$$

The relation between τ and w_n is plotted in Figure 2(a) for various values of α/EI and $\nu = 0.5$. The critical load is the minimum τ that exists and can be expressed by $d\tau/dw_n = 0$. By differentiating the above equations by w_n and setting $d\tau/dw_n = 0$, it can be shown that

$$(w_n - \tau)^2(4EIw_n - (4EI - 3GJ)\tau) = 0, \tag{41}$$

or

$$(w_n + \tau)^2(4EIw_n + (4EI - 3GJ)\tau) = 0. \tag{42}$$

Solving these equations and using $EI = (1 + \nu)GJ$, the critical load and the corresponding wave number can be obtained as

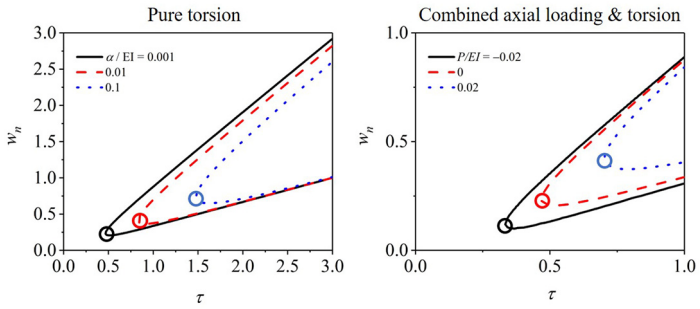

Figure 2. (a) Relation between w_n and $\tau = T/GJ$ at the buckling of a rod under pure torsion. Parameters used are: $\nu = 0.5$ and $\alpha/EI = 0.001,\ 0.01$, and 0.1. (b) Relation between w_n and τ at the buckling of a rod under combined axial loading and torsion. Parameters used are: $\nu = 0.5$, $\alpha/EI = 0.001$, and $P/EI = -0.02,\ 0$, and 0.02. Circles represent the critical or minimum buckling load τ and the corresponding w_n.

$$\tau = \pm \frac{4}{3^{3/4}} \left(\frac{\alpha}{EI}\right)^{1/4} (1+\nu), \tag{43}$$

and

$$w_n = \frac{(1+4\nu)}{3^{3/4}} \left(\frac{\alpha}{EI}\right)^{1/4}. \tag{44}$$

It should be noted that $\tau = \pm w_n$ are also solutions of Equations (41) and (42), respectively. These solutions indicate the trivial case of a straight line. From the above results, the critical τ depends on the stiffness ratio α/EI and the rod's Poisson ratio ν.

2.3.3 Rod buckling under combined axial force and torsional moment. Consider next the general case: the rod is under a combined axial force and torsional moment. Equations (34) and (35) can be written as

$$\alpha + (\tau - w_n)^3((EI - GJ)\tau - EIw_n) + P(\tau - w_n)^2 = 0, \tag{45}$$

or

$$\alpha + (\tau + w_n)^3((EI - GJ)\tau + EIw_n) + P(\tau + w_n)^2 = 0. \tag{46}$$

The relation between τ and w_n is plotted in Figure 2(b) for different values of P/EI. Differentiating the above equation by w_n and setting $d\tau/dw_n = 0$, the following can be obtained

$$(-w_n + \tau)(2(P + 2EIw_n{}^2) + (-8EIw_n + 3GJw_n)\tau + (4EI - 3GJ)\tau^2) = 0, \tag{47}$$

or

$$(w_n + \tau)(2(P + 2EIw_n{}^2) + (8EIw_n - 3GJw_n)\tau + (4EI - 3GJ)\tau^2) = 0. \tag{48}$$

Solving the above two equations, the critical loading τ and its corresponding w_n can be obtained. There are four solutions to τ, given by

$$\tau_{1,2} = \pm \frac{1}{3}\sqrt{\frac{2}{3}} \frac{1}{GJ\sqrt{\alpha}} \times \left[-(P^2 + 12EI\alpha)^{3/2} - P(P^2 - 36EI\alpha)\right]^{1/2}, \tag{49}$$

$$\tau_{3,4} = \pm \frac{1}{3}\sqrt{\frac{2}{3}} \frac{1}{GJ\sqrt{\alpha}} \times \left[(P^2 + 12EI\alpha)^{3/2} - P(P^2 - 36EI\alpha)\right]^{1/2}, \tag{50}$$

while there are two solutions to the wave number:

$$w_{1,2} = \frac{(8EI - 3GJ)\tau \pm (9G^2J^2\tau^2 - 32EIP)^{1/2}}{8EI}. \tag{51}$$

If τ is plotted against P, Equations (49) and (50) give the critical buckling curves. For each τ, Equation (51) gives the corresponding mode wave numbers. Furthermore, Equations (49) and (50) can be non-dimensionalized in the following manner. Define the dimensionless axial load and dimensionless torque as

$$\bar{P} = \frac{P}{(\alpha EI)^{1/2}}, \quad \bar{T} = \frac{T}{(\alpha E^3 I^3)^{1/4}}, \tag{52}$$

where $T = \tau GJ$. Introducing these dimensionless variables into Equations (49) and (50) yields

$$\bar{T}_{1,2} = \pm \frac{1}{3}\left(\frac{2}{3}\right)^{1/2} \sqrt{-(\bar{P}^2 + 12)^{3/2} - \bar{P}(\bar{P}^2 - 36)}, \tag{53}$$

$$\bar{T}_{3,4} = \pm \frac{1}{3}\left(\frac{2}{3}\right)^{1/2} \sqrt{(\bar{P}^2 + 12)^{3/2} - \bar{P}(\bar{P}^2 - 36)}, \tag{54}$$

where $\bar{T}_{1,2}$ are purely imaginary and $\bar{T}_{3,4}$ are purely real as shown next. If the expression under the square root sign in Equation (54) is positive, then $\bar{T}_{3,4}$ are purely real:

$$\begin{aligned} &(\bar{P}^2 + 12)^{3/2} - \bar{P}(\bar{P}^2 - 36) \geqslant 0, \\ &\text{or} \\ &(\bar{P}^2 + 12)^{3/2} \geqslant \bar{P}(\bar{P}^2 - 36). \end{aligned} \tag{55}$$

Squaring both sides of the second expression in Equation (55), it can be reduced to

$$108(\bar{P}^2 - 4)^2 \geqslant 0, \tag{56}$$

which is certainly true. Hence, $\bar{T}_{3,4}$ are purely real. Similarly, it can be shown that $\bar{T}_{1,2}$ are purely imaginary and therefore dismissed as solutions.

The wave numbers can also be non-dimensionalized by substituting the variables $\bar{P}$ and $\bar{T}$ as defined in Equation (52) into Equation (51), leading to

$$\bar{w}_{1,2} = \left(\nu + \frac{5}{8}\right)\bar{T} \pm \frac{1}{8}(9\bar{T}^2 - 32\bar{P})^{1/2}, \tag{57}$$

where

$$\bar{w}_{1,2} = \frac{w_{1,2}}{(\alpha/EI)^{1/4}}. \tag{58}$$

The second derivatives of the magnitude of τ with respect to w_n are given in Appendix A3. Numerical tests show that the second derivatives are always positive for the four sets of real solutions. This indicates the four sets of real solutions are minima.

In the special case of a rod buckling under combined P and T without a surrounding elastic medium, $\alpha = 0$. Applying $T = GJ\tau$, Equations (49)–(51) reduce to

$$P = \frac{T^2}{4EI} \quad \text{and} \quad w_n = (1 + 2\nu)\sqrt{\frac{P}{EI}}, \tag{59}$$

which agree with the classical results [25, 41].

2.4 Deformed shape

At the bifurcation of the rod deformation (i.e., $\mathrm{Det}(\mathbf{L}) = 0$), the six equations in $\mathbf{Lc} = 0$ contain only five independent equations. By solving the five independent equations, c_2, c_3, c_4, c_5, c_6 can be written in terms of c_1:

$$c_2 = c_1 \frac{\mathrm{i}\left(1 + (1+\nu)^2\bar{T}^2\left(\bar{P} + \nu(1+\nu)\bar{T}^2\right) + \left(\bar{P} + 3(1+\nu)(1+2\nu)\bar{T}^2\right)\bar{w}_n^2 + \bar{w}_n^4\right)}{(1+\nu)\bar{T}\left(2\bar{P} + (1+\nu)(1+4\nu)\bar{T}^2\right)\bar{w}_n + (3+4\nu)\bar{T}\bar{w}_n^3}, \tag{60}$$

$$c_3 = 0, \tag{61}$$

$$c_4 = \sqrt{EI\alpha}c_1 \frac{\mathrm{i}\bar{w}_n\left(1 - (1+\nu)\bar{T}^2\left((-1+\nu)\bar{P} + 3\nu^2(1+\nu)\bar{T}^2\right) + \left(\bar{P} + (3 + 2\nu(3+\nu))\bar{T}^2\right)\bar{w}_n^2 + \bar{w}_n^4\right)}{\bar{T}\left(2(1+\nu)\bar{P} + \left((1+\nu)^2(1+4\nu)\bar{T}^2 + (3+4\nu)\bar{w}_n^2\right)\right)}, \tag{62}$$

$$c_5 = \sqrt{EI\alpha}c_1 \frac{\left(\nu + \nu(1+\nu)^2\bar{T}^2\left(\bar{P} + \nu(1+\nu)\bar{T}^2\right) - \left((2+\nu)\bar{P} + (1 + 3\nu - 2\nu^3)\bar{T}^2\right)\bar{w}_n^2 - 3(1+\nu)\bar{w}_n^4\right)}{2(1+\nu)\bar{P} + \left((1+\nu)^2(1+4\nu)\bar{T}^2 + (3+4\nu)\bar{w}_n^2\right)}, \tag{63}$$

$$c_6 = 0. \tag{64}$$

Substituting the above solutions into Equation (19) and using $\mathbf{d}_3 = \mathbf{d}_3^{(0)} + \varepsilon\mathbf{d}_3^{(1)}$, the real part of $\mathbf{d}_3$ can be obtained as

$$\mathbf{d}_3 = \{c_1 \cos(w_n s)\sin(\tau s) - \gamma c_1 \cos(\tau s)\sin(w_n s),\ -c_1 \cos(w_n s)\cos(\tau s) - \gamma c_1 \sin(\tau s)\sin(w_n s), 1\}, \tag{65}$$

where the dimensionless parameter γ is given by

$$\gamma = \frac{1 + (1+\nu)^2\bar{T}^2\left(\bar{P} + \nu(1+\nu)\bar{T}^2\right) + \left(\bar{P} + 3(1+\nu)(1+2\nu)\bar{T}^2\right)\bar{w}_n^2 + \bar{w}_n^4}{\bar{T}\bar{w}_n\left(2(1+\nu)\bar{P} + (1+\nu)^2(1+4\nu)\bar{T}^2 + (3+4\nu)\bar{w}_n^2\right)}. \tag{66}$$

By Equation (2), the deformed shape $\mathbf{x} = \mathbf{x}^{(0)} + \varepsilon\mathbf{x}^{(1)}$ can then be reconstructed by using $\mathbf{x} = \int \mathbf{d}_3\, ds = \int (\mathbf{d}_3^{(0)} + \varepsilon\mathbf{d}_3^{(1)})\, ds$ as

$$x_1 = -c_1\left(\frac{(\tau + \gamma w_n)}{(\tau - w_n)(\tau + w_n)}\cos(\tau s)\cos(w_n s) + \frac{(\gamma\tau + w_n)}{(\tau - w_n)(\tau + w_n)}\sin(\tau s)\sin(w_n s)\right), \tag{67}$$

$$x_2 = c_1\left(-\frac{(\tau + \gamma w_n)}{(\tau - w_n)(\tau + w_n)}\sin(\tau s)\cos(w_n s) + \frac{(\gamma\tau + w_n)}{(\tau - w_n)(\tau + w_n)}\cos(\tau s)\sin(w_n s)\right), \tag{68}$$

$$x_3 = s. \tag{69}$$

3. Discussion: universal critical buckling curve, mode shapes, and elastic stiffness assumption

Equation (54) is the equation for the *universal* critical buckling curve under combined axial and torsional loads. It predicts the combined $\bar{P}$ and $\bar{T}$ critical values for buckling. No material and geometrical parameters appear explicitly in this equation. Hence, if experiments are performed on rods of various diameters and elastic constants in an elastic medium of various stiffnesses, the results, if non-dimensionalized according to Equation (52), should in theory all collapse into the single universal curve given by Equation (54). This is illustrated in Figure 3. The universal curve may also be useful in material design and selection. Universal relations have been found previously, e.g., a universal surface for planar

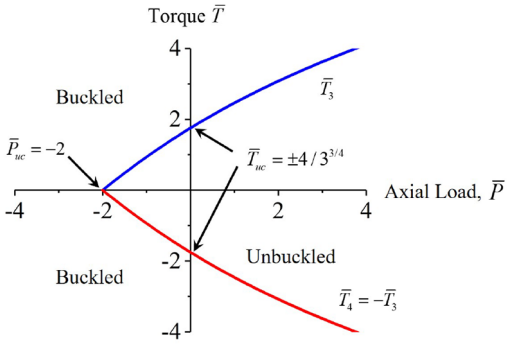

Figure 3. Universal critical bucking curve for combined axial–torsional loads $\bar{P} = P/(\alpha EI)^{1/2}$ and $\bar{T} = T/(\alpha E^3 I^3)^{1/4}$. The curve is independent of material constants and geometry. Note the critical uniaxial compressive load $\bar{P}_{uc} = -2$ and the critical pure torsional load $\bar{T}_{uc} = \pm 4/3^{3/4}$.

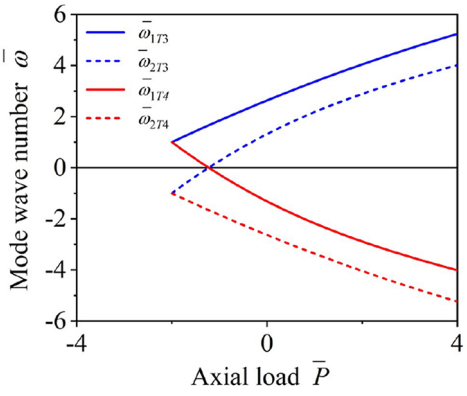

Figure 4. Plot of the non-dimensional mode wave number against the non-dimensional critical axial load. Two different wave numbers are predicted for each torsional load, i.e., $\bar{w}_{1T3}$ and $\bar{w}_{2T3}$ for $\bar{T}_3$, and $\bar{w}_{1T4}$ and $\bar{w}_{2T4}$ for $\bar{T}_4$. Since the two torsional loads are equal and opposite, $\bar{w}_{1T3}$ and $\bar{w}_{2T4}$ (also $\bar{w}_{2T3}$ and $\bar{w}_{1T4}$), produce the same mode shapes of different handedness.

snap conditions was recently described for strips subjected to kinematic conditions at the ends [42], and universal stress–strain relations were also found for nonlinear soft materials [43]. Many choices exist for selecting E, I, and α while ensuring the material system does not buckle under the most severe expected combined loads.

Qualitatively, the universal curve shows that (i) a torque (provided it does not cause buckling itself) always reduces the critical compressive axial load, (ii) a reducing axial compressive load or an increasing axial tensile load increases the critical torque, and (iii) the two branches of the universal curve enclose those $\bar{P}$ and $\bar{T}$ values giving the unbuckled state while exteriorizing those values giving the buckled state. In addition, the universal critical axial load (in the absence of $\bar{T}$) and the universal critical torque (in the absence of $\bar{P}$) for buckling can be determined easily from Equation (54):

$$\bar{P}_{uc} = -2, \quad \bar{T}_{uc} = \pm \frac{4}{3^{3/4}} \approx \pm 1.7548. \tag{70}$$

Equation (70) reveals that the critical uniaxial compression load is twice $(\alpha EI)^{1/2}$, which may be interpreted as a coupled elastic parameter incorporating the stiffness α of the surrounding medium and the bending rigidity EI of the elastic rod. Furthermore, the critical torque for buckling is 1.7548 times $(\alpha E^3 I^3)^{1/4}$. Hence, increasing the stiffness of the surrounding medium enhances the critical compressive load more than the critical torque, while increasing the bending rigidity of the rod enhances the critical torque more than the critical compressive load. As a further remark, one can also define the non-

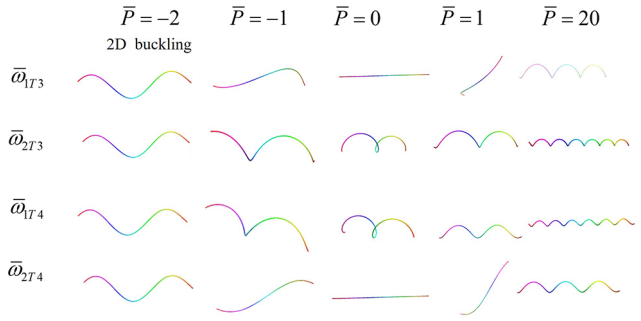

Figure 5. Possible mode shapes under various axial loads $\bar{P}=-2,\ -1, 0, 1, 20$ (with corresponding critical $\bar{T}$). In general, two different mode shapes (row 1 and row 2, or row 3 and row 4 with different handedness) are predicted for each critical load combination.

dimensional loads $\bar{\bar{P}}=\bar{P}/|\bar{P}_{uc}|$, $\bar{\bar{T}}=\bar{T}/|\bar{T}_{uc}|$ and the corresponding universal curve relating $\bar{\bar{T}}$ and $\bar{\bar{P}}$ would then pass through the points $(-1, 0)$ and $(0, \pm 1)$.

Substituting $\bar{T}_3$ of Equation (54) into Equation (57), $\bar{w}_{1,2}$ can now be plotted as $\bar{w}_{1T3}$, $\bar{w}_{2T3}$ versus $\bar{P}$ (in blue full and dashed lines). Similarly, if $\bar{T}_4$ (which is $-\bar{T}_3$) is substituted instead, $\bar{w}_{1T4}$, $\bar{w}_{2T4}$ can be plotted versus $\bar{P}$ (in red full and dashed lines). These four curves are shown in Figure 4 for $\nu=0.3$. Although independent of geometry, they are dependent on the Poisson's ratio. Hence, they are not truly universal curves. For uniaxial compression (without torque), $\bar{P}_{uc}=-2$ and there are two mode wave numbers which are equal and opposite to each other. Under combined axial load and torque, there are also two possible wave numbers for each torque, i.e., $\bar{w}_{1T3}$ and $\bar{w}_{2T3}$ for $\bar{T}_3$, and $\bar{w}_{1T4}$ and $\bar{w}_{2T4}$ for $\bar{T}_4$. Here, $\bar{w}_{1T3}$ and $\bar{w}_{2T4}$ produce the same mode shapes of different handedness. The same can be said for $\bar{w}_{2T3}$ and $\bar{w}_{1T4}$. However, the two wave number groups are different from each other.

Figure 5 shows the mode shapes for $\bar{P}=-2,\ -1, 0, 1, 20$ (with corresponding critical $\bar{T}$), for the following parameter values $\alpha/EI=0.001$ and $\nu=0.5$. As examples, the mode shapes are constructed using the real part of $\mathbf{x}$ as shown in Equations (67)–(69). In the case of uniaxial compression $\bar{P}=-2$, the mode shape is two-dimensional. For other cases, the shapes are three-dimensional as shown in Figure 5. For $\bar{P}=0$, one of the shapes is straight and the other is a helical shape. The shapes in row 1 and row 4, and row 2 and row 3, are the same but with different handedness. The realization of the actual mode shape will depend on the boundary conditions and the associated energy state of the mode.

Several forms of the relation between the parameter α and the elastic properties of a linear elastic matrix have been presented. For example, by treating the force on the medium generated by the rod as a sum of point-like forces and using the principle of superposition, α in both the transverse ($\alpha_\perp$) and longitudinal ($\alpha_\parallel$) direction were derived as [10]: $\alpha_\perp=2\alpha_\parallel\approx 4\pi G/\ln(L/a)$, where L is the wavelength and a the rod radius. But these expressions were obtained on the basis of several assumptions and an overall uncertainty in the gel spring constant was estimated to be ~50%. Similarly, in [17] the authors used the same form for the transverse and longitudinal couplings. However, the wavelength L in these expressions could not be determined *a priori*. Instead of using the wavelength L, in [44] the authors used the length of the rod l, i.e., $\alpha_\perp=2\alpha_\parallel\approx 4\pi G/\ln(l/a)$. In all these forms, the longitudinal coupling $\alpha_\parallel$ is half the transverse coupling $\alpha_\perp$. Furthermore, the coupling in the longitudinal direction was neglected in some works. In [3], the microtubules were assumed to deform only in the lateral direction and the longitudinal force between rod and matrix was neglected. The transverse coupling used was $\alpha_\perp=4\pi G/\ln(L/a)$. In [45], $\alpha_\perp$ was estimated to be $2.8\pi G$, and the effect of longitudinal direction was also neglected. In our work, we assume the coupling parameters to be the same in all directions. However, the solution of x_3 in Equation (69) shows a null component along the x_3 direction, which means that the effect of $\alpha_\parallel$ is negligible, at least to the first order.

4. Conclusion

The buckling of a long elastic rod embedded in an elastic medium and subjected to combined axial and torsional loads has been investigated by means of a perturbation approach. The effect of the

surrounding medium on the rod buckling is incorporated through a response force, characterized by the stiffness of the medium.

The main, and previously unavailable, result is an analytical expression connecting the critical axial load, both in compression and tension, to the critical torsional load. This expression allows the demarcation of the axial–torsional load space into regions of buckled and unbuckled states. The possible corresponding mode wave numbers are also predicted. A second significant result is the nondimensionalization of the critical axial and torsional loads, leading to a universal relationship independent of material and geometry. This has advantages in analyzing experiments with rods of various elastic constants and with surrounding media of various stiffnesses, as well as for material design purposes. The analytical expression also reveals that a reducing axial compression or an increasing axial tension enhances the critical torsional load for buckling. Finally, the mode shapes are generally three-dimensional, with two possible mode wave numbers predicted for each critical axial–torsional load combination.

Conflict of interest

The author(s) declared no potential conflicts of interest with respect to the research, authorship, and/or publication of this article.

Funding

The author(s) received no financial support for the research, authorship, and/or publication of this article.

ORCID iDs

Dong Wang https://orcid.org/0000-0002-8569-8713
Mao See Wu https://orcid.org/0000-0001-7448-0826

References

[1] van Loenhout, MT, de Grunt, M, and Dekker, C. Dynamics of DNA supercoils. *Science* 2012; 338(6103): 94–97.
[2] Watson, JD, and Crick, FH. Molecular structure of nucleic acids. *Nature* 1953; 171(4356): 737–738.
[3] Brangwynne, CP, MacKintosh, FC, Kumar, S, et al. Microtubules can bear enhanced compressive loads in living cells because of lateral reinforcement. *J Cell Biol* 2006; 173(5): 733–741.
[4] Fletcher, DA, and Mullins, RD. Cell mechanics and the cytoskeleton. *Nature* 2010; 463(7280): 485.
[5] Jiang, H, and Zhang, J. Mechanics of microtubule buckling supported by cytoplasm. *J Appl Mech* 2008; 75(6): 061019.
[6] Li, T. A mechanics model of microtubule buckling in living cells. *J Biomech* 2008; 41(8): 1722–1729.
[7] Wang, C, Ru, C, and Mioduchowski, A. Orthotropic elastic shell model for buckling of microtubules. *Phys Rev E* 2006; 74(5): 052901.
[8] Mendelson, NH. Helical bacillus subtilis macrofibers: morphogenesis of a bacterial multicellular macroorganism. *Proc Natl Acad Sci* 1978; 75(5): 2478–2482.
[9] Mendelson, N. Bacterial macrofibres: the morphogenesis of complex multicellular bacterial forms. *Sci Prog* 1990; 74(296 Pt 4): 425–441.
[10] Silverberg, JL, Noar, RD, Packer, MS, et al. 3D imaging and mechanical modeling of helical buckling in Medicago truncatula plant roots. *Proc Natl Acad Sci* 2012; 109(42): 16794–16799.
[11] Kringelbach, ML, Jenkinson, N, Owen, SL, et al. Translational principles of deep brain stimulation. *Nat Rev Neurosci* 2007; 8(8): 623.
[12] Santillan, ST, Virgin, LN, and Plaut, RH. Static and dynamic behavior of highly deformed risers and pipelines. *J Offshore Mech Arctic Eng* 2010; 132(2): 021401.
[13] Wang, L, Shi, R, Yuan, F, et al. Global buckling of pipelines in the vertical plane with a soft seabed. *Appl Ocean Res* 2011; 33(2): 130–136.
[14] Dogterom, M, and Yurke, B. Measurement of the force–velocity relation for growing microtubules. *Science* 1997; 278(5339): 856–860.
[15] Wang, N, Naruse, K, Stamenović, D, et al. Mechanical behavior in living cells consistent with the tensegrity model. *Proc Natl Acad Sci* 2001; 98(14): 7765–7770.
[16] Brodland, G, and Gordon, R. Intermediate filaments may prevent buckling of compressively loaded microtubules. *J Biomech Eng* 1990; 112(3): 319–321.
[17] Das, M, Levine, AJ, and MacKintosh, F. Buckling and force propagation along intracellular microtubules. *Europhys Lett* 2008; 84(1): 18003.

[18] Su, T, Liu, J, Terwagne, D, et al. Buckling of an elastic rod embedded on an elastomeric matrix: planar vs. non-planar configurations. *Soft Matter* 2014; 10(33): 6294–6302.
[19] Lim, S. Dynamics of an open elastic rod with intrinsic curvature and twist in a viscous fluid. *Phys Fluids* 2010; 22(2): 024104.
[20] Wang, Z, and van der Heijden, G. Localised lateral buckling of partially embedded subsea pipelines with nonlinear soil resistance. *Thin-Walled Struct* 2017; 120: 408–420.
[21] Nelson, P. Transport of torsional stress in DNA. *Proc Natl Acad Sci* 1999; 96(25): 14342–14347.
[22] Lazarus, C, Soheilypour, M, and Mofrad, MR. Torsional behavior of axonal microtubule bundles. *Biophys J* 2015; 109(2): 231–239.
[23] Yi, L, Chang, T, and Ru, C. Buckling of microtubules under bending and torsion. *J Appl Phys* 2008; 103(10): 103516.
[24] Gong, S, and Xu, P. Influences of pipe–soil interaction on dynamic behaviour of deepwater s-lay pipeline under random sea states. *Ships Offshore Struct* 2017; 12(3): 370–387.
[25] Love, AEH. *A Treatise on the Mathematical Theory of Elasticity*. Cambridge: Cambridge University Press, 2013.
[26] Thompson, JMT, and Champneys, A. From helix to localized writhing in the torsional post-buckling of elastic rods. *Proc R Soc Lond A* 1996; 452(1944): 117–138.
[27] Timoshenko, SP, and Gere, JM. *Theory of Elastic Stability*. New York: McGraw-Hill, 1961.
[28] Valverde, J, and Van der Heijden, G. Magnetically-induced buckling of a whirling conducting rod with applications to electrodynamic space tethers. *J Nonlin Sci* 2010; 20(3): 309–339.
[29] Valverde, J, and van der Heijden, G. Helical buckling of a whirling conducting rod in a uniform magnetic field. *Int J Non-Lin Mech* 2012; 47(3): 38–53.
[30] Goriely, A, and Tabor, M. The nonlinear dynamics of filaments. *Nonlin Dynam* 2000; 21(1): 101–133.
[31] Euler, L. *Methodus inveniendi lineas curvas maximi minimive proprietate gaudentes*. apud Marcum-Michaelem Bousquet, 1744.
[32] Lagrange, J. Sur la figure des colonnes. *Miscellanea Taurinensia* 1770; 5: 123–166.
[33] Antman, SS. *Nonlinear Problems of Elasticity*. New York: Springer, 2005.
[34] Ciarletta, P, and Destrade, M. Torsion instability of soft solid cylinders. *IMA J Appl Math* 2014; 79(5): 804–819.
[35] Goriely, A, Vandiver, R, and Destrade, M. Nonlinear euler buckling. *Proc R Soc A Math Phys Eng Sci* 2008; 464(2099): 3003–3019.
[36] Kabir, AMR, Inoue, D, Afrin, T, et al. Buckling of microtubules on a 2D elastic medium. *Scientific Rep* 2015; 5: 17222.
[37] Wang, Z, van der Heijden, G, and Tang, Y. Localised upheaval buckling of buried subsea pipelines. *Marine Struct* 2018; 60: 165–185.
[38] Zhou, H, and Ou-Yang, ZC. Spontaneous curvature-induced dynamical instability of Kirchhoff filaments: application to DNA kink deformations. *J Chem Phys* 1999; 110(2): 1247–1251.
[39] Landau, L, and Lifshitz, E. *Theory of Elasticity*. 3rd Ed. Oxford: Pergamon Press, 1986.
[40] Liu, J, Huang, J, Su, T, et al. Structural transition from helices to hemihelices. *PLoS One* 2014; 9(4): e93183.
[41] Van der Heijden, G, and Thompson, J. Helical and localised buckling in twisted rods: a unified analysis of the symmetric case. *Nonlin Dyn* 2000; 21(1): 71–99.
[42] Cazzolli, A, and Dal Corso, F. Snapping of elastic strips with controlled ends. *Int J Solids Struct* 2019; 162: 285–303.
[43] Wang, D, and Wu, MS. Second-order elasticity of soft multilayer capsules: universal relations and parametric studies. *Int J Eng Sci* 2013; 73: 17–32.
[44] Shan, W, Chen, Z, Broedersz, C, et al. Attenuated short wavelength buckling and force propagation in a biopolymer-reinforced rod. *Soft Matter* 2013; 9(1): 194–199.
[45] O'Keeffe, SG, Moulton, DE, Waters, SL, et al. Growth-induced axial buckling of a slender elastic filament embedded in an isotropic elastic matrix. *Int J Non-Lin Mech* 2013; 56: 94–104.

Appendices

A1. Expressions for F_{21}, F_{31}, F_{12}, F_{32}, F_{13}, F_{23} and G_{21}, G_{31}, G_{12}, G_{32}, G_{13}, G_{23}

The terms F_{21}, F_{31} and G_{21}, G_{31} in Equation (12) are combinations of $f_1, f_2, f_3, \kappa_1, \kappa_2, \kappa_3$ and their derivatives. Specifically, they can be expressed as

$$F_{21} = \kappa_2 f_1{}' - \kappa_1 f_2{}' + \kappa_2{}' f_1 - f_3{}'', \tag{A1}$$

$$F_{31} = \kappa_3 f_1{}' - \kappa_1 f_3{}' + \kappa_3{}' f_1 + f_2{}'', \tag{A2}$$

$$G_{21} = \kappa_1{}^2 \kappa_3 + \kappa_2{}^2 \kappa_3 + \kappa_3{}^2 + 2\kappa_1{}' \kappa_2 + \kappa_1 \kappa_2{}' - \kappa_3{}'', \tag{A3}$$

$$G_{31} = -\kappa_1{}^2 \kappa_2 - \kappa_3{}^2 \kappa_2 - \kappa_2{}^3 + 2\kappa_1{}' \kappa_3 + \kappa_1 \kappa_3{}' + \kappa_2{}'', \tag{A4}$$

Similarly, F_{12}, F_{32} and G_{12}, G_{32} in Equation (13) can be expressed as

$$F_{12} = \kappa_1 f_2^{'} - \kappa_2 f_1^{'} + \kappa_1^{'} f_2 + f_3^{''}, \tag{A5}$$

$$F_{32} = \kappa_3 f_2^{'} - \kappa_2 f_3^{'} + \kappa_3^{'} f_2 - f_1^{''}, \tag{A6}$$

$$G_{12} = -\kappa_1{}^2\kappa_3 - \kappa_2{}^2\kappa_3 - \kappa_3{}^3 + \kappa_1{}^{'}\kappa_2 + 2\kappa_1\kappa_2{}^{'} + \kappa_3{}^{''}, \tag{A7}$$

$$G_{32} = \kappa_2{}^2\kappa_1 + \kappa_3{}^2\kappa_1 + \kappa_1{}^3 + 2\kappa_2{}^{'}\kappa_3 + \kappa_2\kappa_3{}^{'} - \kappa_1{}^{''}. \tag{A8}$$

In addition, F_{13}, F_{23} and G_{13}, G_{23} in Equation (14) can be expressed as

$$F_{13} = \kappa_1 f_3^{'} - \kappa_3 f_1^{'} + \kappa_1^{'} f_3 - f_2^{''}, \tag{A9}$$

$$F_{23} = \kappa_2 f_3^{'} - \kappa_3 f_2^{'} + \kappa_2^{'} f_3 + f_1^{''}, \tag{A10}$$

$$G_{13} = \kappa_1{}^2\kappa_2 + \kappa_3{}^2\kappa_2 + \kappa_2{}^3 + 2\kappa_3{}^{'}\kappa_1 + \kappa_3\kappa_1{}^{'} - \kappa_2{}^{''}, \tag{A11}$$

$$G_{23} = -\kappa_2{}^2\kappa_1 - \kappa_3{}^2\kappa_1 - \kappa_1{}^3 + 2\kappa_3{}^{'}\kappa_2 + \kappa_3\kappa_2{}^{'} + \kappa_1{}^{''}, \tag{A12}$$

It can be seen that $F_{21}, F_{31}, F_{12}, F_{32}, F_{13}, F_{23}$ in these equations contain coupled terms such as $\kappa_2 f_1^{'}$, $\kappa_2^{'} f_1$, etc., whereas $G_{21}, G_{31}, G_{12}, G_{32}, G_{13}, G_{23}$ contain only the curvatures and their derivatives.

A2. Derivation of $\mathbf{K}$

The zeroth- and first-order terms of $\kappa_1, \kappa_2, \kappa_3$ are derived here. By using Equations (20) and (24), $\mathbf{B}$ up to the first order of ε can be written as

$$\mathbf{B} = \mathbf{I} + \varepsilon\mathbf{A} = \begin{pmatrix} 1 & 0 & 0 \\ 0 & 1 & 0 \\ 0 & 0 & 1 \end{pmatrix} + \varepsilon \begin{pmatrix} 0 & \beta_3 & -\beta_2 \\ -\beta_3 & 0 & \beta_1 \\ \beta_2 & -\beta_1 & 0 \end{pmatrix} = \begin{pmatrix} 1 & c_3 e^{isw_n}\varepsilon & -c_2 e^{isw_n}\varepsilon \\ -c_3 e^{isw_n}\varepsilon & 1 & c_1 e^{isw_n}\varepsilon \\ c_2 e^{isw_n}\varepsilon & -c_1 e^{isw_n}\varepsilon & 1 \end{pmatrix}, \tag{A13}$$

and

$$\frac{\partial \mathbf{B}}{\partial s} = \begin{pmatrix} 0 & ic_3 e^{isw_n} w_n \varepsilon & -ic_2 e^{isw_n} w_n \varepsilon \\ -ic_3 e^{isw_n} w_n \varepsilon & 0 & ic_1 e^{isw_n} w_n \varepsilon \\ ic_2 e^{isw_n} w_n \varepsilon & -ic_1 e^{isw_n} w_n \varepsilon & 0 \end{pmatrix}. \tag{A14}$$

Substituting Equations (23) and (24) into Equation (21), $\mathbf{K}$ up to first order can be obtained as

$$\begin{aligned} \mathbf{K} = \mathbf{K}^{(0)} + \mathbf{K}^{(1)} &= \begin{pmatrix} 0 & \kappa_3^{(0)} & -\kappa_2^{(0)} \\ -\kappa_3^{(0)} & 0 & \kappa_1^{(0)} \\ \kappa_2^{(0)} & -\kappa_1^{(0)} & 0 \end{pmatrix} + \begin{pmatrix} 0 & \kappa_3^{(1)} & -\kappa_2^{(1)} \\ -\kappa_3^{(1)} & 0 & \kappa_1^{(1)} \\ \kappa_2^{(1)} & -\kappa_1^{(1)} & 0 \end{pmatrix} = \begin{pmatrix} 0 & \tau & 0 \\ -\tau & 0 & 0 \\ 0 & 0 & 0 \end{pmatrix} \\ &+ \varepsilon \begin{pmatrix} 0 & ic_3 e^{isw_n} w_n & -ic_2 e^{isw_n} w_n \\ -ic_3 e^{isw_n} w_n & 0 & ic_1 e^{isw_n} w_n \\ ic_2 e^{isw_n} w_n & -ic_1 e^{isw_n} w_n & 0 \end{pmatrix}. \end{aligned} \tag{A15}$$

It should be noted that the linearization of the six nonlinear Equations (12)–(17) can also be done in terms of $(\kappa_1^{(1)}, \kappa_2^{(1)}, \kappa_3^{(1)}, f_1^{(1)}, f_2^{(1)}, f_3^{(1)})$, which could make the derivation of the critical buckling load easier. However, in order to obtain the mode shape, we performed the linearization in terms of $(\beta^{(1)}, \beta_2^{(1)}, \beta_3^{(1)}, f_1^{(1)}, f_2^{(1)}, f_3^{(1)})$.

A3. Second-order derivatives

The second-order derivative condition is checked to ensure that the critical loadings obtained are minima.

Case (1) Rod buckling under pure axial loading. The second derivative of the magnitude of P with respect to w_n at critical buckling is

$$\frac{d^2P}{dw_n^2}\left(w_n=\left(\frac{\alpha}{EI}\right)^{1/4}\right)=8EI>0. \tag{A16}$$

Case (2) Rod buckling under pure torsion. The second-order derivative of the magnitude of τ with respect to w_n at critical buckling is

$$\frac{d^2\tau}{dw_n^2}=\frac{4(1+\nu)}{\left(\frac{3\alpha}{EI}\right)^{1/4}}>0. \tag{A17}$$

Case (3) Rod buckling under combined axial force and torsional moment. For a fix P, the second-order derivative of τ with respect to w_n at critical buckling can be obtained as

$$\frac{d^2\tau}{dw_n{}^2}=\frac{1}{-\tau+w_n}+\frac{2(GJ-4EI)\tau+(8EI+GJ)w_n}{2P+(4EI-GJ)w_n^2-(8EI-5GJ)w_n\tau+4(EI-GJ)\tau^2}, \tag{A18}$$

or

$$\frac{d^2\tau}{dw_n{}^2}=-\frac{1}{\tau+w_n}+\frac{2(GJ-4EI)\tau-(8EI+GJ)w_n}{2P+(4EI-GJ)\tau^2+(8EI-5GJ)w_n\tau+4(EI-GJ)w_n^2}. \tag{A19}$$

Substituting the critical value for τ and w_n in Equations (50) and (51) into the above expressions, the second-order derivatives can be expressed as a function of applied force P and material properties E, ν, and α. The expression is complex and difficult to theoretically verify its sign. However, we have carried out many numerical tests by choosing different values of P, E, ν, and α. All of the results show that the second-order derivatives of the magnitude of τ with respect to w_n for all four sets of solutions are always positive. Hence, the four sets of solutions represent minima.